3

Dimensional Metrology and Frequency Sweeping Interferometry

Alexandre Cabral, José Manuel Rebordão and Manuel Abreu
Faculty of Sciences, Physics Department and Centre for Astronomy and Astrophysics of the University of Lisbon, University of Lisbon, Portugal

1. Introduction

Absolute distance metrology is needed for a wide gamut of applications with different ranges and resolutions. One good example is space missions requiring independent satellites working cooperatively: the management of such formations requires several levels of metrology to keep the formation coherent and to enable guidance and navigation of the complete formation (Calvel et al., 2004). Beyond a certain level of accuracy, at the end of the metrology chain, optical metrology becomes mandatory to achieve the required high accuracy.

Optical metrology is normally used to describe the measurement of some physical parameter using optical methods. Almost all of the technical fields we can think of make use of optical metrology. A good example is the use of interferometry to achieve high accuracy in length measurements. Optical interferometry relies on the phenomenon of interference between light waves to make extremely accurate measurements. In 1887, Michelson, along with physicist Edward W. Morley, set up an experiment to determine if the speed of light was dependent on the speed of the observer. According to the accepted theory of that time, light had to propagate in a medium called the ether. The motion of Earth travelling through the ether would affect the fringe pattern on Michelson's interferometer, because it would take the light longer to travel over one arm than the other arm. When the interferometer was rotated through 90°, the fringes would shift if the speed of light was not constant. In this most celebrated null experiment in the history of science, Michelson and Morley observed no changes in the fringes after many repetitions. The speed of light appeared to be constant, regardless of the speed of its source, a fact that was later explained by Einstein's theory of relativity.

The "failure" of the Michelson-Morley experiment was the seed of the new science of interferometry. The improved device used in the Michelson-Morley experiment was one of the first interferometers, and Michelson, who had always an intense passion for accuracy in measurement, quickly recognized his invention's potential for highly accurate instrumentation.

Since its debut, the interferometer (Fig. 1) has undergone a number of modifications and has been specialized for use in a variety of fields. In 1895, Michelson used it to measure the International Prototype Metre in Paris in units of wavelength (Michelson & Benoit, 1985).

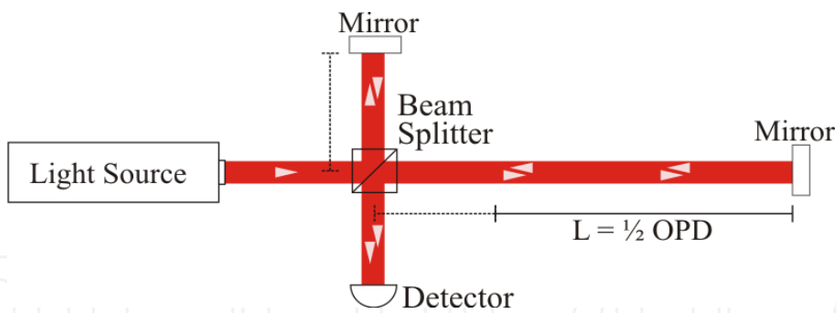

Fig. 1. Setup of a Michelson interferometer.

Michelson's contributions to interferometry, from 1880 to 1930, dominated the field to such extent that optical Interferometry was regarded for many years as a closed chapter. However, the last few decades have seen an explosive growth of interest in interferometry due to several new developments, mainly associated to the light source. The improvement of frequency stabilised lasers, of frequency tunable lasers and, lately, the appearance of femtosecond lasers have encouraged the use of the interferometer in dimensional metrology. In addition, nanometre-level interferometry with low-coherence sources has also created a plethora of additional metrological applications and technological developments. Interferometry is still alive in the XXI century.

Coherent absolute distance metrology is one of the most interesting techniques for dimensional metrology. Without movement of the mirror that define the Optical Path Difference (OPD) in the interferometer, measurements are made without ambiguity, by using either one or several synthetic wavelengths resulting from the beating of two or more wavelengths (multiple wavelength interferometry) or, in the case of frequency sweeping interferometry, from an optical frequency sweep.

Frequency Sweeping Interferometry (FSI) based sensors are relatively simple devices and can fulfil an important role in dimensional metrology. In addition, their parameterisation flexibility allows various tradeoffs to be performed, either technology driven or application related.

The generation of the synthetic wavelength in FSI is based on optical frequency sweeping the laser source within a given sweep range. As frequency sweeps, detection electronics counts synthetic wavelength maxima (temporal "synthetic fringes") without ambiguity. Its sensitivity to variations of distance (drift) during the sweep limits the maximum resolution to a few micrometres. FSI does not require stabilised or well known laser sources and relies only on a tunable laser and a frequency sweep range measurement subsystem (for example, based on a Fabry-Pérot interferometer). FSI sensor complexity can be tuned to system specifications – when requirements are modest, FSI complexity is reduced accordingly.

In the last years, FSI has seen a considerable development and several solutions have been presented. The most important are based only upon a tunable laser and a frequency measurement sub-system, systems built around both a reference and a measurement interferometer, or based on the use of an additional stabilized laser, some developed for high accuracy under special controlled laboratory conditions, others driven by robustness in

uncontrolled environments (Kinder & Salewski, 2002; Cabral & Rebordão, 2005; Swinkels et al., 2005; Yang et al., 2005). An example is the Dual FSI concept, conceived to overcome the decrease in accuracy as the measurement range increases, as a consequence of the uncertainty propagation in the synthetic wavelength measurement. To overcome this problem, in order to maintain the low complexity associated to short distances, in Dual FSI the measurement process for larger ranges is reduced to the close range case, by increasing the reference arm with a long reference fibre and using an ancillary interferometer to measure (calibrate) continuously the fibre length.

2. Absolute Distance Measurement by optical interferometry

Absolute Distance Measurements (ADM) can be performed by several optical methods. Generally, one has non-interferometric methods for large ranges with moderate accuracies and interferometric methods for high accuracies and moderate ranges, limited by the coherence length of the source. ADM can also be performed on the basis of low-coherence or white light interferometry but, in this case, the measuring range is limited to a few millimetres. Lately, the measuring range of interferometric methods increased due to the increase of the coherence length and the development on new coherent sources.

ADM interferometric techniques are typically based on the use of multiple or time varying wavelength sources. Single wavelength interferometry is a powerful tool in displacement measurement when high accuracy is required, however, as a major drawback, is only applicable to relative measurements. To measure an absolute distance it is necessary to use incremental interferometry: to measure a displacement it is necessary to fix a reference position and to carefully displace a suitable reflector from that position to the final one, and basically counting each interferometer fringe event. This must be done avoiding any optical misalignment that would result in a loss of the interference signal and therefore of the measure.

Multiple Wavelength Interferometry (MWI) is a technique were the use of (at least) two different wavelengths allows the generation of a synthetic wavelength much longer than the two individual optical wavelengths, actually increasing the non-ambiguity range (NAR) for interferometry (Dändliker et al., 1988; Dändliker et al., 1995). In MWI, each synthetic wavelength (one or several) is generated using two different and very accurately known optical wavelengths. By selecting a small synthetic wavelength it is possible to achieve high resolution (at the micrometre level or even smaller). However the intrinsic ambiguity of the measurement limits the measurement range. To overcome the ambiguity, a chain of increasing synthetic wavelengths is generated (or a combination with another sensor) to cover the required range (Salvadé et al., 2000). For large ranges, several wavelengths are required and MWI can become indeed a very complex solution.

In a first approach, FSI is equivalent to MWI. In FSI, the generation of the synthetic wavelength is based on frequency sweeping the laser source within a given sweep range. The technique is not new, has strong similarities to radar, dating back to the 80's (Kikuta et al., 1986), but it was not studied extensively until the development of tunable lasers and the emergence of External Cavity Diode Lasers (ECDL) (Hecht, 2001). As frequency sweeps, detection electronics counts synthetic wavelength fringes (temporal "synthetic fringes")

without ambiguity, thus making it particularly interesting for large measurement ranges (Thiel et al., 1995; Stone, 1999; Edwards et al., 2000; Coe et al., 2004; Cabral & Rebordão, 2005; Swinkels et al., 2005). While in Double Wave interferometry (DWI) – which is a particular case of MWI - we have a fixed synthetic wavelength, while in FSI, as the frequency is being swept, the value of the synthetic wavelength is decreasing down to a value defined by the total sweep range.

In contrast to MWI, FSI does not require independent stabilized and well known laser sources and relies only on a tunable laser and a frequency sweep range measurement subsystem, normally based on a Fabry-Pérot interferometer (FP).

As in DWI, the synthetic wavelength Λ is inversely proportional to the frequency sweep range $\Delta\nu$ (see next section). While in MWI we measure only the fractional part of the synthetic wavelength fringe, in FSI both the fractional and integer number of synthetic fringes can be measured. Thus, the absolute value of the OPD (between the two arms of a Michelson interferometer) will be determined without ambiguity.

It is not possible to elaborate an objective comparison between different techniques without an a priori definition of the sensor requirements: maximum range, accuracy, technological complexity, reliability, cost, etc. Nevertheless, a trade-off between the two basic methods, FSI and MWI, can be done in a qualitative way, considering the three main parameters: measurement distance, measurement uncertainty and overall complexity of the sensor subsystem.

FSI main advantage is the capability to perform large range measurements due to the non-ambiguity nature of the technique, limited only by the coherence length of the tunable laser (a few hundred metres). FSI main drawback is the sensitivity to drift that, even with a compensation method, will limit the accuracy at the micrometre level. With an affordable complexity in the frequency sweeping (i.e. synthetic wavelength) measurement sub-system, for large distances, FSI can achieve a relative accuracy around 10^{-5}. With a high degree of complexity (locking the laser to a resonant cavity) accuracies can be improved by one or two orders of magnitude.

3. Frequency Sweeping Interferometry

In the previous section it was mentioned that the intensity detected in a Michelson interferometer changes with the OPD change for a fixed laser frequency. If the frequency changes in time, the detected intensity will change not only due to the OPD change but also due to the frequency change.

FSI is based in the variation of the optical frequency ν, or angular frequency $\omega = 2\pi\nu$, of a tunable laser in a Michelson interferometer. In this situation, the frequency no longer represents the periodical property of the wave, and in this case, the phase component is a non-linear function of time. Defining the instantaneous angular frequency as the derivative of the phase:

$$\omega(t) = \frac{d\phi(t)}{dt} \tag{1}$$

the phase is given by:

$$\phi(t) = \int_0^t \omega(t)dt + \varphi_0 \tag{2}$$

where φ_0 is the initial phase of the light source. The electric-field amplitude (not considering its spatial variation) is then described by:

$$E(t) = A(t)e^{i\varphi(t)} \tag{3}$$

If two optical waves are derived from the same coherent light source, the angular frequency changing linearly in time (during the measurement period) but travel along different paths and are recombined at a point in space to interfere, the detected signal will change in time, unlike the case of a fixed frequency. In a Michelson interferometer, the angular frequency of the reference wave within the time interval $t \in [0, \Delta t]$ is given by:

$$\omega_R(t) = \Omega \cdot t + \omega_0 \tag{4}$$

where ω_0 is the angular frequency at the beginning of the frequency sweep, and Ω is the angular frequency sweep rate. If the angular frequency variation has a linear behaviour, the value of the angular frequency sweep rate is given by:

$$\Omega = 2\pi \frac{\Delta\nu}{\Delta t} \tag{5}$$

where $\Delta\nu$ is the frequency sweep range. The phase of the reference wave is given by:

$$\varphi_R(t) = \frac{1}{2}\Omega \cdot t^2 + \omega_0 \cdot t + \varphi_0 \tag{6}$$

The wave function of the reference electric field is described by:

$$E_R(t) = A_R \cdot e^{i\left[\frac{1}{2}\Omega t^2 + \omega_0 t + \varphi_0\right]} \tag{7}$$

where A_R is the amplitude of the reference wave (considered to be constant in time). The signal wave, travelling in the other arm of the interferometer, can be described similarly:

$$\omega_S(t) = \Omega \cdot (t + \tau) + \omega_0 \tag{8}$$

$$\varphi_R(t) = \frac{1}{2}\Omega \cdot (t + \tau)^2 + \omega_0 \cdot (t + \tau) + \varphi_0 \tag{9}$$

$$E_S(t) = A_S \cdot e^{i\left[\frac{1}{2}\Omega(t+\tau)^2 + \omega_0(t+\tau) + \varphi_0\right]} \tag{10}$$

where A_S is the amplitude of the signal wave (considered to be constant in time) and τ is the delay time of the signal wave with respect to the reference wave. The delay is related to the OPD in the interferometer by:

$$\tau = \frac{n \cdot OPD}{c} \tag{11}$$

where n is the refractive index of the optical propagation medium. When these two waves interfere, the intensity of the resulting electrical field can be written as:

$$\begin{aligned} I &= \left\langle \left|\mathbf{E}_R\right|^2 \right\rangle + \left\langle \left|\mathbf{E}_S\right|^2 \right\rangle + \left\langle \left|\mathbf{E}_R \cdot \mathbf{E}_S^*\right| \right\rangle + \left\langle \left|\mathbf{E}_R^* \cdot \mathbf{E}_S\right| \right\rangle \\ I(\tau,t) &= \left|A_R\right|^2 + \left|A_S\right|^2 + 2\left(A_R \cdot A_S\right)\cos\left(\Omega \cdot \tau \cdot t + \omega_0 \cdot \tau + \frac{1}{2} \cdot \Omega \cdot \tau^2\right) \end{aligned} \tag{12}$$

or equivalently by:

$$\begin{aligned} I(\tau,t) &= I_R + I_S + 2\sqrt{I_R I_S} \cdot \cos\left(\Omega \cdot \tau \cdot t + \omega_0 \cdot \tau + \frac{1}{2} \cdot \Omega \cdot \tau^2\right) \\ &= I_0\left[1 + V \cdot \cos\left(\Omega \cdot \tau \cdot t + \omega_0 \cdot \tau + \frac{1}{2} \cdot \Omega \cdot \tau^2\right)\right] \end{aligned} \tag{13}$$

where I_R and I_S are the intensities of the reference and signal wave, I_0 is the average intensity and V is the visibility (or contrast) of the signal:

$$V = \frac{2\sqrt{I_R I_S}}{I_R + I_S} \tag{14}$$

The relative importance of the different terms of the cosine argument in Eq.(13) depends on τ, Ω and ω_0. The most relevant parameter is the delay τ. This value is limited by the coherence length of the tunable laser. For a coherence length of a few hundred metres, $\tau < 1$ µs, the value of $\frac{1}{2}.\Omega.\tau^2$ will be several orders of magnitude lower than the other two terms (a typical value for Ω is 10^4 GHz/s). It is thus conceivable to neglect the term $\frac{1}{2}.\Omega.\tau^2$ in Eq.(13), and simplify the equation:

$$I(\tau,t) = I_0\left[1 + V \cdot \cos\left(\Omega \cdot \tau \cdot t + \omega_0 \cdot \tau\right)\right] \tag{15}$$

If we rewrite Eq.(15) considering the optical frequency and the OPD to describe the optical waves and the interference phenomena, we obtain (from Eq.(5) and (11)):

$$I(OPD(t),t) = I_0\left[1 + V \cdot \cos\left(2\pi\left(\frac{\Delta\nu}{c} \cdot n \cdot OPD(t) \cdot \frac{t}{\Delta t} + \frac{n \cdot OPD(t)}{\lambda}\right)\right)\right] \tag{16}$$

where *OPD(t)* represents the OPD variation during the sweep and λ is the optical wavelength (in vacuum) at the beginning of the sweep. Defining a synthetic wavelength Λ, inversely proportional to the frequency sweep range, by:

$$\Lambda = \frac{c}{\Delta\nu} \tag{17}$$

Eq.(16) becomes:

$$I\left(OPD(t),t\right)=I_0\left[1+V\cdot\cos\left(2\pi\left(\frac{n\cdot OPD(t)}{\Lambda}\cdot\frac{t}{\Delta t}+\frac{n\cdot OPD(t)}{\lambda}\right)\right)\right] \tag{18}$$

It is clear that the value of the OPD can contribute to the detected signal both in terms of the optical wavelength λ and/or in terms of the synthetic wavelength Λ generated by the frequency sweep.

To analyse Eq.(18) we consider two simple cases: 1 - no frequency sweep and, 2 - static OPD. In the first case, $\Delta\nu = 0$, $\Lambda = \infty$ and Eq.(18) becomes:

$$I\left(OPD(t),t;\Delta\nu=0\right)=I_0\left[1+V\cdot\cos\left(2\pi\left(\frac{n\cdot OPD(t)}{\lambda}\right)\right)\right] \tag{19}$$

In this case, as the OPD changes in time, detector will sense a complete fringe for every λ/n variation in the OPD. This is the particular case of relative single wavelength interferometry.

In the second case, the OPD is constant during the frequency sweep, and Eq.(18) becomes:

$$I\left(OPD_0,t\right)=I_0\left[1+V\cdot\cos\left(2\pi\left(\frac{n\cdot OPD_0}{\Lambda}\cdot\frac{t}{\Delta t}+\frac{n\cdot OPD_0}{\lambda}\right)\right)\right] \tag{20}$$

The second term of the cosine argument represents only a constant phase and, as the frequency sweeps, the detector will sense a number of synthetic fringes that correspond to the absolute value of the OPD in Λ/n units. This is the ideal baseline for FSI. The absolute value of a distance L (half the OPD) in a FSI Michelson interferometer (Fig. 1) is obtained from the detected signal during the sweep interval Δt by:

$$L=\frac{N}{2}\cdot\frac{\Lambda}{n} \tag{21}$$

where N is the number of synthetic fringes detected from the beginning to the end of the sweep (integer and fractional part).

However, a third more realist case must be considered when the two phenomena, frequency sweep and OPD variation, occur simultaneously. In this case, the contribution of the two phenomena is mixed up in the detected signal, and it is impossible to distinguish between the individual contributions from each one of them.

It must be emphasised that, for a typical ADM application, the absolute value of the length to be measured is always several orders of magnitude larger than the length variations during the sweep (hereafter designated by drift). When drift occurs during the frequency sweep, two different types of fringes will be generated:

1. synthetic wavelength fringes (Λ-fringes) due to frequency sweep;
2. optical wavelength fringes (λ-fringes) due to changes in distance caused by drift.

As it is impossible to distinguish these two types of fringes, λ-fringes will be misinterpreted as Λ-fringes, causing the noise error (drift) to be multiplied by a large amplification factor Λ/λ.

The effect of drift in the FSI measurement can be separated in two different cases. If the drift signal (movement direction) changes during the sweep duration (usually less than a second), we are in presence of a low amplitude drift typically with frequencies identical or higher than the measurement frequency. In this case, the small amplitudes will have a smaller influence and, if it is not negligible, due to its random nature, it can be reduced applying a mean filter to the measurements.

In a second case, if the drift signal does not change during the sweep, we are in the presence of a low frequency drift with considerable amplitude even within the small time duration of the sweep (bearing in mind that this effect will be amplified). In this case, the drift must be compensated. Independent relative metrology and control can always reduce the drift by measuring it and by actuating a delay line during the sweep, or take it into account in the distance calculations. Nevertheless, this option would increase the complexity of the sensor, jeopardizing one of the FSI advantages.

If the OPD is written as:

$$OPD(t) = 2 \cdot \left(L_0 + l(t)\right) \tag{22}$$

where L_0 is the distance at the beginning of the frequency sweep and $l(t)$ the relative distance variation in time, the drift (the factor of 2 is due to the round trip in the measuring arm of the interferometer), the detected intensity will be given by:

$$I(t) = I_0\left[1 + V \cdot \cos\left(2\pi\left(\frac{n \cdot 2 \cdot \left(L_0 + l(t)\right)}{\Lambda} \cdot \frac{t}{\Delta t} + \frac{n \cdot 2 \cdot \left(L_0 + l(t)\right)}{\lambda}\right)\right)\right] \tag{23}$$

The absolute distance measurement is based on the fringe counting from the beginning ($t = 0$) to the end of the frequency sweep ($t = \Delta t$). As long as the drift signal does not change during the sweep, it is not important to know how the fringes change in time but only to measure the total number of detected fringes from the start to the end of the sweep. For this purpose, we need only to describe the drift as:

$$l(t) = \begin{cases} 0 & \text{for } t = 0 \\ \Delta L & \text{for } t = \Delta t \end{cases} \tag{24}$$

From Eq.(23) and (24) we can determine the number of detected fringes by subtracting the initial from the final phase of the cosine argument (divided by 2π):

$$N = \left[\frac{n \cdot 2 \cdot \left(L_0 + \Delta L\right)}{\Lambda} + \frac{n \cdot 2 \cdot \left(L_0 + \Delta L\right)}{\lambda}\right]_{t=\Delta t} - \left[\frac{n \cdot 2 \cdot \left(L_0\right)}{\lambda}\right]_{t=0} \tag{25}$$

resulting in:

$$N = \frac{2 \cdot n}{\Lambda}\left(L_0 + \left(1 + \frac{\Lambda}{\lambda}\right) \cdot \Delta L\right) \tag{26}$$

From Eq.(26) it is possible to determine the absolute distance at the end of the sweep:

$$L = N\frac{\Lambda}{2\cdot n} - \frac{\Lambda}{\lambda}\cdot \Delta L \tag{27}$$

Comparing Eq.(27) and (21), it is clear that the drift introduces an error equal to the drift amplitude multiplied by an amplification factor given by the ratio between synthetic and optical wavelengths.

When drift is neglected, compensation is not performed and the second term of Eq.(27) corresponds to an additional error in the measurement. As an example, for a sweep range of 50 GHz ($\Lambda \approx 6$ mm) in the visible ($\lambda \approx 600$ nm), the amplification factor is ≈ 10 000; a drift with an amplitude of 1 nm would introduce an error of 10 μm in the measurement. Depending on requirements, such an error may or may not be negligible.

It is thus very important to work with the lowest possible amplification factor either by using a longer laser wavelength (near IR) or a smaller synthetic wavelength by increasing the sweep range (without increasing the sweep duration otherwise the drift would also increase). Nevertheless, special care must be taken when the synthetic wavelength decreases, because the number of synthetic fringes will increase (which may also increase the complexity of the electronics counting subsystem).

3.1 Synthetic wavelength measurement and distance calculation

To calculate the absolute distance it is necessary to know not only the number of fringes but also the value of the synthetic wavelength, by measuring the value of the frequency sweep range.

In the experimental examples that will be discussed, the frequency sweep range measurement subsystem is based on a Fabry-Pérot interferometer (FP). The sweep range measurement is obtained by multiplying the FP free spectral range (FSR) by the number of resonances detected while the laser frequency sweeps. The beginning of the sweep is determined by a particular cavity mode; the laser sweeps from mode to mode and resonances, separated by the FP FSR, are detected and counted (Fig. 2). The frequency sweep range is then given by:

$$\Delta\nu = r\cdot FSR \tag{28}$$

where r is the number of detected FSR (number of resonances minus one).

From Eq.(17) and (28) we obtain:

$$\Lambda = \frac{c}{r\cdot FSR} \tag{29}$$

The measured length is, considering Eq.(27) and (29), given by:

$$L = N\frac{c}{2\cdot n\cdot r\cdot FSR} - \frac{c}{\lambda\cdot r\cdot FSR}\cdot \Delta L \tag{30}$$

Without drift, or when its influence is smaller than the required uncertainty, we are in a Static Mode and the absolute distance can be calculated simply from:

$$L = N \frac{c}{2 \cdot n \cdot r \cdot FSR} \tag{31}$$

where c, n and FSR are constants and N and r are the variables to be measured.

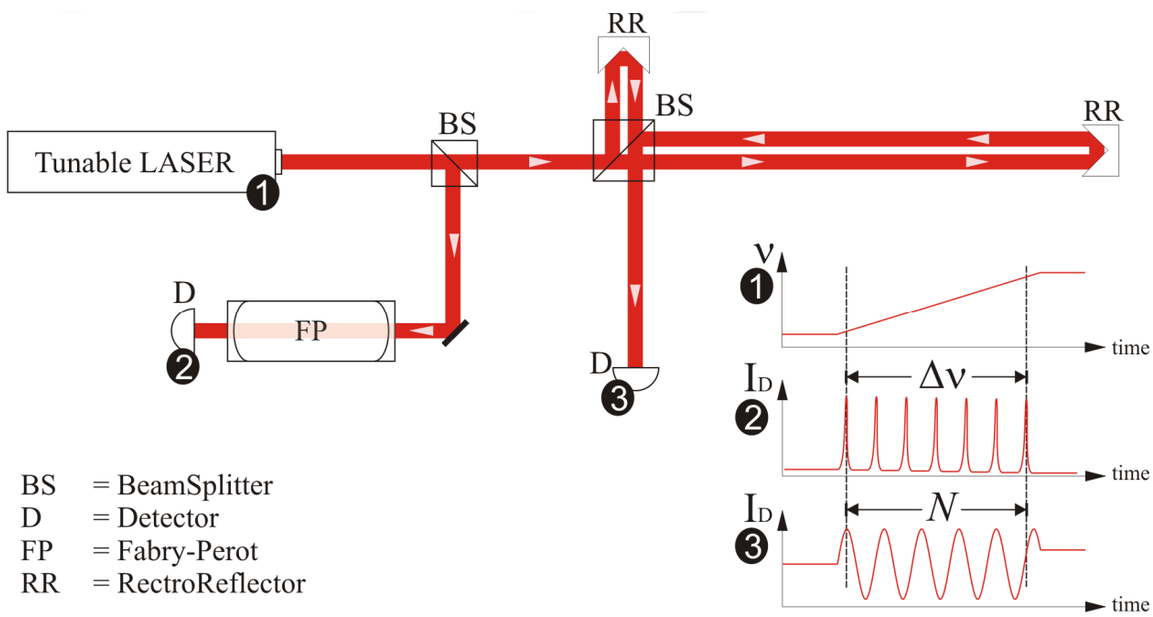

Fig. 2. FSI Setup. While the laser sweeps the frequency, the interferometer detector acquires the fringes and a FP measures the sweep range by counting the resonances of the cavity.

3.2 Drift compensation method for dynamic mode measurements

When it is not realistic to assume that the distance under measurement is constant during the sweep, the drift effect on the measurement has to be compensated. If we can assume that during the sweep there is no acceleration, i.e. the drift speed is constant, it is possible to remove the drift influence from two consecutive measurements with different values of sweep duration or/and sweep range. For a constant drift speed S_{drift}, the drift amplitude is described by:

$$\Delta L = S_{drift} \cdot \Delta t \tag{32}$$

and Eq.(27) can be written as:

$$L = N \frac{\Lambda}{2 \cdot n} - \text{sign}(\Delta\nu) \cdot \frac{\Lambda}{\lambda} \cdot S_{drift} \cdot \Delta t \tag{33}$$

where sign(Δν) is the sign of the frequency variation (+ for an increasing and - for a decreasing frequency sweep). For two consecutive measurements, 1 and 2, the following system of equations holds:

$$\begin{cases} L_1 = N_1 \dfrac{\Lambda_1}{2 \cdot n} - \text{sign}(\Delta\nu_1) \cdot \dfrac{\Lambda_1}{\lambda} \cdot S_{drift} \cdot \Delta t_1 \\ L_2 = N_2 \dfrac{\Lambda_2}{2 \cdot n} - \text{sign}(\Delta\nu_2) \cdot \dfrac{\Lambda_2}{\lambda} \cdot S_{drift} \cdot \Delta t_2 \\ L_2 = L_1 + S_{drift} \cdot \Delta t_3 \end{cases} \tag{34}$$

where Δt_3 represents the time interval between the end of the first and the end of the second measurements. Drift speed and the corrected absolute distance for the second measurement are recovered by inverting Eq.(34) and using Eq.(29):

$$\begin{cases} S_{drift} = \dfrac{\lambda}{2 \cdot n} \cdot \dfrac{\left(\dfrac{N_2}{r_2} - \dfrac{N_1}{r_1} \right)}{\left(\Delta t_3 \cdot \dfrac{FSR}{c} \cdot \lambda \right) + \left(\text{sign}(\Delta\nu_2) \dfrac{\Delta t_2}{r_2} - \text{sign}(\Delta\nu_1) \dfrac{\Delta t_1}{r_1} \right)} \\ L_2 = \dfrac{c}{r_2 \cdot FSR} \cdot \left(\dfrac{N_2}{2 \cdot n} \text{-sign}(\Delta\nu_2) \cdot S_{drift} \cdot \dfrac{\Delta t_2}{\lambda} \right) \end{cases} \tag{35}$$

These equations are exact as long as drift speed is constant for the time span of the two measurements. Note that the frequency of the dynamic mode measurement can still be the same as it would be in the static mode single measurement as the first measurement can always be the same as the second measurement of the previous pair of sweeps. Thus, every new measurement enables another dynamic mode measurement (in this case, the characteristics of the two sweeps would swap from measurement to measurement).

The most simple implementation of this compensation method is to use two consecutive measurements with different signs on the sweep range ($\Delta\nu$) and equal durations, corresponding to a symmetrical triangular shaped frequency sweep ($\Delta t_2 = \Delta t_1 = \Delta t$ and $\Delta\nu_2 = -\Delta\nu_1 = \Delta\nu \Rightarrow r_2 = r_1 = r$). In this case, we obtain:

$$\begin{cases} S_{drift} = \dfrac{\lambda}{2 \cdot n} \cdot \dfrac{N_2 - N_1}{\left(\Delta t_3 \cdot \dfrac{r \cdot FSR}{c} \cdot \lambda \right) - 2\Delta t} \\ L_2 = \dfrac{c}{r \cdot FSR} \cdot \left(\dfrac{N_2}{2 \cdot n} + \cdot S_{drift} \cdot \dfrac{\Delta t}{\lambda} \right) \end{cases} \tag{36}$$

With this approach, we are not only correcting the length measurement but also providing a measurement of the drift speed.

3.3 Measurement performances

FSI sensor performance does not depend on the stability of the absolute value of the frequency but on the uncertainty in the frequency sweep range: there is no need to calibrate the system for absolute frequencies.

The system final uncertainty has two major contributors:

- uncertainty in the measured number of fringes N (the synthetic fringe interpolation uncertainty);
- uncertainty in the sweep range measurement Δv. The later depends on:
  - uncertainties in the FSR value and on
  - determination of the number of detected FSR (r).

Without drift (static mode), the final uncertainty, corresponding to a coverage probability of approximately 95% (IOS, 1995), can be obtained from (31):

$$\delta L = \sqrt{\sum_i \left(\frac{\partial L(X_i)}{\partial X_i} \cdot \delta X_i \right)^2}$$

$$\delta L = \sqrt{\begin{array}{l} \left(\frac{c}{2 \cdot n \cdot FSR \cdot r} \cdot \delta N \right)^2 + \\ \left(\frac{c \cdot N}{2 \cdot n \cdot FSR^2 \cdot r} \cdot \delta FSR \right)^2 + \left(\frac{c \cdot N}{2 \cdot n \cdot FSR \cdot r^2} \cdot \delta r \right)^2 + \\ \left(\frac{c \cdot N}{2 \cdot n^2 \cdot FSR \cdot r} \cdot \delta n \right)^2 \end{array}} \tag{37}$$

The uncertainty component in N is only the fringe phase uncertainty, δN, because the integer number of fringes can be considered to be measured exactly. In the determination of the integer part, if a fringe is missed or over counted, the effect is easily noticed and can be corrected using simple outlier removal procedures. This uncertainty does not change with range, and depends only on the value of the synthetic wavelength. This component is dominant for small distances because it does not increase with L.

The next two components, in r and in FSR, determine the uncertainty in the sweep range measurement and are related to the FP performances.

The uncertainty in r depends on FP finesse and on the capability of the signal processing to localize resonance maxima. In order to locate resonance maxima in time unambiguously, the maxima of the signal generated by the FP should be clearly discriminated. The higher the finesse, the easier it is to locate accurately each resonance maxima in time and, therefore, reduce derived sensor errors.

The value of the FSR uncertainty is determined by the FP calibration and stability. The stability depends on length and optical variations induced by temperature and misalignments. For high resolution (low FSR uncertainty), thermal stabilization and low-thermal expansion materials may be required.

In contrast to the uncertainty in the synthetic fringe interpolation, the uncertainty components related to the sweep range measurement increase with range. These components become dominant for large distances.

The refractive index of air contributes to the measurement uncertainty due to the instabilities in the optical medium caused by the variations of the air temperature, pressure

and humidity. The value of the refractive index of air can be determined by the Edlén equation (Stone & Zimmerman, 2004). The different parameters contribute differently to the index uncertainty. As an example, for normal laboratory conditions (p = 100,4 kPa; T = 20 °C; RH = 50%), the contribution given by a change in the humidity of 50% is equivalent to a change of 0,2 kPa or 0,5 °C. The influence of the humidity is thus irrelevant compared to the influence of pressure and temperature. In order to neglect the contribution of the laboratory environment the refractive index contribution should be kept at least around 10^{-6}. This can be achieved by measuring the pressure with an uncertainty around ±0,2 kPa (±2 mbar) and by measuring (and controlling) the temperature within ±0,5 °C. Note that for a space application this factor in null.

Fig. 3 shows an example of the system performances for these three components as a function of distance, considering typical parameters (presented in Table 1) used in the experimental results to shown later.

The value of the PF FSR should be selected in order to optimize its contribution to the final uncertainty. For the same sweep range, the number of resonances decreases when the FSR increases. Thus, if the δFSR contribution is larger than the δr contribution, the value of the FSR should increase and vice-versa. It must be noted that a low FSR is limited by the maximum available etalon length (the length of the FP increases when the FSR decreases) and by the FSR uncertainty (as the FSR becomes smaller, the number of resonances for the same sweep range increases and the contribution of the FSR uncertainty increases as well).

The previous analysis corresponds to a driftless static mode. In the dynamic mode with a constant drift speed, the same analysis can be performed starting with Eq. (35) or (36), leading in this case to a more complex solution. Nevertheless, the conclusions are basically the same.

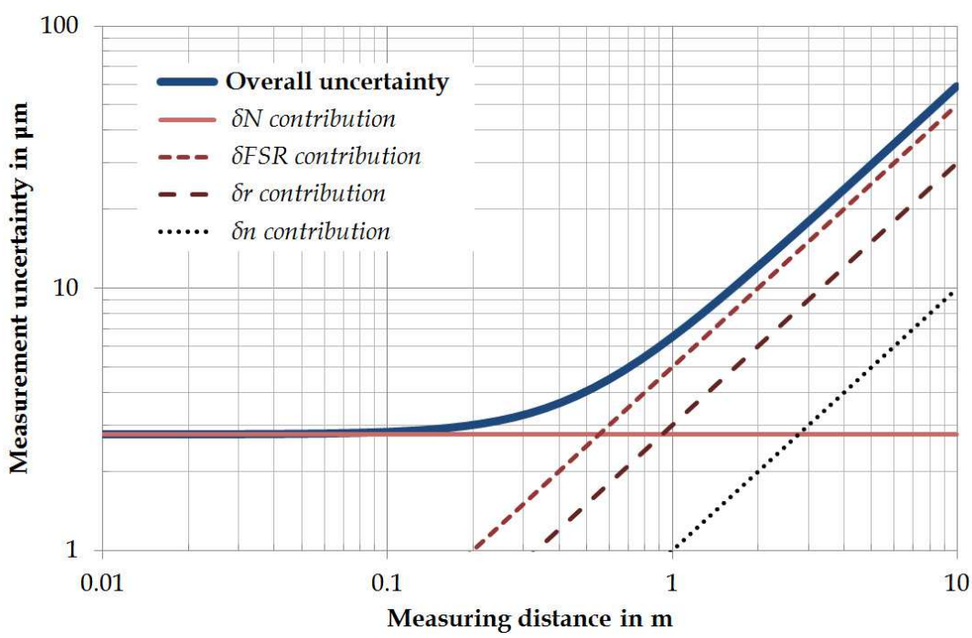

Fig. 3. Example of the FSI model, considering typical parameters presented in Table 1. (δN = 1/360 of a fringe, $\delta FSR = 5.10^{-6}$, $\delta r = 3.10^{-6}$, $\delta n = 1.10^{-6}$).

Parameter	*Value*	*Uncertainty*
Frequency sweep range	$\Delta\nu$ = 150 GHz	$\delta\Delta\nu$ = 750 kHz 5.10^{-6} Hz/Hz
Synthetic wavelength	Λ = 2 mm	$\delta\Lambda$ = 10 nm 5.10^{-6} m/m
Synthetic fringes		δN = 1/360
FP FSR	FSR = 1 GHz	δFSR = 5 kHz 5.10^{-6} Hz/Hz
Number of FSR	r = 150	$\delta r = 3.10^{-6}$
Refractive index	n = 1,00027	$\delta n = 1.10^{-6}$

Table 1. FSI parameters used in the simulation presented in Fig. 3.

4. Dual FSI concept for large range measurements

As mentioned before, as we increase the measurement range, accuracy and complexity are typically linked together. This is due to the fact that in FSI the measurement uncertainty increases with distance, as a consequence of the uncertainty propagation of the synthetic wavelength measurement (directly related to the FP performance). In order to achieve the required uncertainty one would have to increase the FP stability (thermal and mechanical) and improve the calibration and resonance detection characteristics (i.e. using Pound-Drever-Hall technique to lock the laser into FP resonances). As a consequence, the expected impact on sensor complexity would be critical. For large ranges, this increase in uncertainty can be considered the main drawback of the technique.

To overcome this problem, maintaining the low complexity associated to short distances, the measurement process for larger ranges can be reduced to the close range case, by limiting the OPD in the interferometer. This can be achieved by increasing the reference arm with a long reference fibre and introducing the concept of dual FSI mode, where an ancillary interferometer is used to measure (calibrate) continuously the fibre length (Cabral et al, 2009).

By adding a long reference fibre in the reference arm, the measured OPD is reduced to the real distance minus half fibre optical path length. Using an additional interferometer, the fibre is calibrated with the same accuracy but with lower requirements. This assumes that the fibre length is constant, during a certain time interval, and therefore the calibration will be the result of averaging for that period (uncertainty is reduced by a factor proportional to the square root of the number of measurements).

In this dual FSI approach, the final uncertainty is the sum of two components:

- uncertainty in the measurement of the reduced OPD (twice the absolute distance minus Reference Fibre length);
- calibration uncertainty of the Reference Fibre Optical Path Length (OPL);

In addition, during the calibration period, we must guarantee that the change in fibre OPL due to thermal variation is negligible compared with the required calibration uncertainty. It must be noted that the change in fibre length due to thermal variation is not the only limiting factor to the number of measurements that can be averaged for fibre calibration. Beyond a certain reduction factor, i.e. after a certain averaging period, the uncertainty

component related to the FP FSR calibration uncertainty becomes dominant and there is no benefit in increasing the calibration period.

Besides the measurement dispersion, there are other uncertainty components that can influence the final measurement accuracy. The resolution in the fringe phase and resonance position measurements is currently much smaller than the measurement dispersion, and thus its contribution is not significant. The uncertainty in the calibration of the FP FSR is the most important one for large distance measurements in a single FSI configuration but, in the dual approach, it is possible to achieve a very small contribution considering the value of the dispersion component.

In order to maintain low hardware complexity, the optical setup for the implementation of this Dual FSI concept makes use of the same laser and FP for the two interferometers, and also some common beam splitters (BS). For that, a Mach-Zehnder configuration was selected, and is presented in Fig. 4, where the two interferometers are shown separately (note that BS1, BS2 and the reference fibre are common to both interferometers).

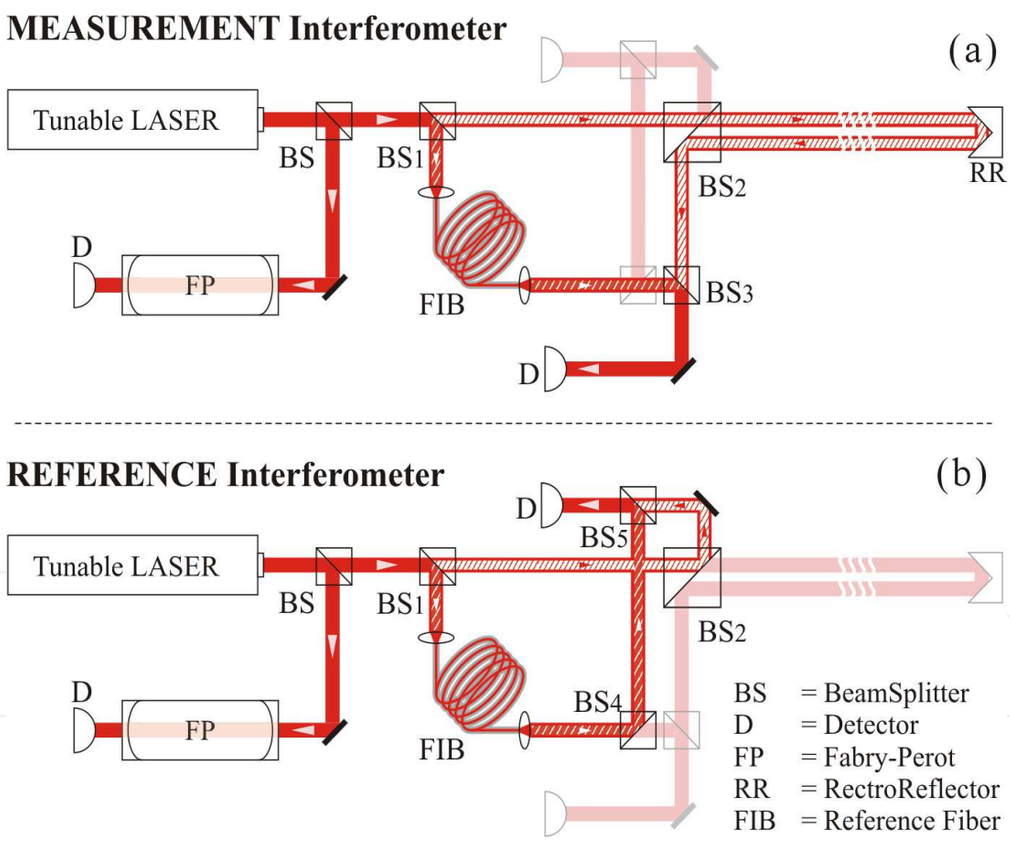

Fig. 4. Dual FSI interferometers setup, measurement (a) and reference (b).

The measurement interferometer evaluates the OPD between the OPL of twice the distance in measurement (due to the round trip) and the OPL added by the reference fibre, as shown in Fig. 4(a). The reference interferometer, shown in the Fig. 4(b), will measure the OPL added by the reference fibre that cause the reduction of the OPD in the measurement interferometer.

5. Experimental implementation of FSI based sensors

In order to demonstrate the capabilities of FSI based sensors, two implementations are described in this section, one for FSI and another for Dual FSI, both tailored for space applications (i.e. long distances, no atmosphere refraction errors are considered, specific operational requirements associated to measurement rate and accuracy).

The first absolute distance sensor, based in FSI, was designed for a space mission comprising a multiple aperture optical telescope (coherent array), to measure the OPD between two sub-telescopes and the combining-telescope with an uncertainty at the 10 µm level at a 10 Hz measurement rate with the lowest possible technical complexity.

The second sensor, based in Dual FSI, was defined in view of a coronagraph mission composed of two spacecraft in a free-flying formation. The requirements on the absolute distance metrology sensor prototype were a measurement uncertainty below the 100 µm level for a distance around 50 m at a 10 Hz measurement rate.

In both sensors, the Laser and the FP are the key items. Complex tasks normally implemented in real time electronics were assigned to data processing, thus moving system complexity to the software area.

A drift compensation model using consecutive measurements was implemented and validated experimentally. Fig. 5 shows the principle behind the compensation technique using two consecutive measurements with different signs on the sweep range ($\Delta\nu$) and equal durations, corresponding to a symmetrical triangular shaped frequency sweep ($\Delta t_2 = \Delta t_1 = \Delta t$ and $\Delta\nu_2 = -\Delta\nu_1 = \Delta\nu \Rightarrow r_2 = r_1 = r$).

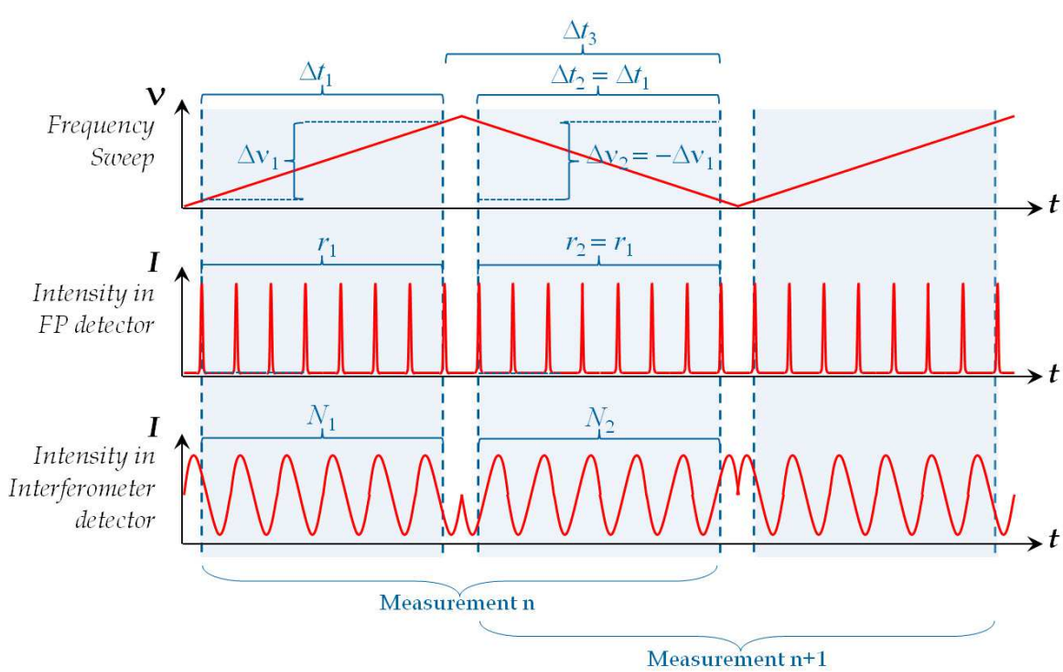

Fig. 5. Principle of the Drift compensation model using two consecutive measurements with different signs on the sweep range and equal durations corresponding to a symmetrical triangular shaped frequency sweep.

Note that the frequency of the dynamic mode measurement can still be the same as it would be in the static mode single measurement as the first measurement can always be the same as the second measurement of the previous pair of sweeps. Thus, every new measurement enables another dynamic mode measurement (in this case, the characteristics of the two sweeps would swap from measurement to measurement). With this approach, we are not only correcting the length measurement but also providing a measurement of the drift speed, using Eq.(36).

5.1 Tunable laser

FSI needs a tunable laser, the frequency of which changes continuously without mode hop. The tunable range should be able to cover several tens of GHz, and this range must be completely swept in a time frame not exceeding a tenth of second. Laser linewidth must be small in order to generate a coherence length of several tens of metre. It is also important to have a compact, robust and with low complexity laser.

Although several options exist to provide wavelength/frequency tuning, the best solution to cope with the requirements is an External Cavity Diode Laser (ECDL) (Amann & Buus, 1998). Traditional diode-laser technology provides high reliability, high electrical efficiency, and a wide range of available wavelengths. By using an external cavity built around a diode laser, it is possible to achieve single-mode operation with narrow linewidth and precise frequency tuning. The extended cavity leads to a spectral narrowing of the laser output to below 1 MHz. The coherence length can thus be in the order of a few hundred metres.

5.2 Fabry-Pérot interferometer

In FSI implementation described, the frequency sweep range measurement subsystem is based on a FP interferometer (Vaughan, 1989). As the sweep range measurement is obtained by multiplying the FP FSR by the number of resonances detected while the laser frequency sweeps, the FP interferometer is a critical component of the sensor.

A FP is a linear resonator which consists of two highly reflecting mirrors forming a standing-wave cavity. In this case, we exploit the fact that the transmission through such a cavity exhibits sharp resonances, making it perfect as a frequency reference cavity.

Two basic types of FP cavity exist: planar and confocal. The confocal is more appropriate for the current application as it has inherent higher finesse, is much less sensitive to mirror misalignment (because it is not critical to maintain mirror parallelism), and for the same FSR the length of the confocal cavity is half the length of the planar cavity. When a confocal FP is illuminated by a monochromatic beam close to the axis, a multiple beam interference pattern is produced near the centre of the interferometer. At precisely the confocal spacing, each mirror images the other back upon itself so that a paraxial ray is re-entrant after four traversals of the cavity. This means that the transmitted spectrum is reproduced with every quarter wavelength change in the mirror separation. Consequently, the FSR is given by:

$$FSR = \frac{c}{4 \cdot n \cdot d} \tag{38}$$

where c is the speed of light, n is the refractive index of the optical medium between the mirrors, and d is the distance between the spherical mirrors (whose radius of curvature is equal to the spacing between them).

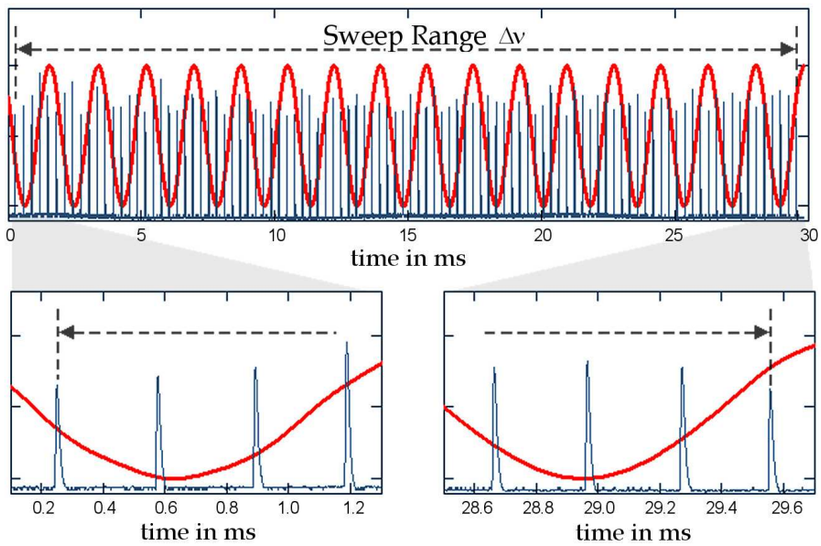

Fig. 6. Typical FSI range and, consecutively, the frequency sweep range value and its uncertainty.

5.3 Data processing

The data acquisition of the FSI interferometer is based in a simple homodyne detection scheme. During the measurement, while the laser frequency is sweeping, signals from the detectors of the FP and interferometer (one or two depending if it is FSI or Dual FSI) are acquired simultaneously. As the maximum number of fringes for the required range is small, it is conceivable to acquire all the data for subsequent processing. After signal processing, we obtain the number of fringes per resonance N/r.

As the requirements on the sampling rate of the data acquisition subsystem increase, the system should be able to keep only the initial and final parts of the signal with high resolution and acquire the middle data at a lower sampling rate - system performances depend only on the accurate determination of the initial and final resonances and zero crossing positions (another possibility is to lock the laser frequency to the initial and final resonances, although this solution increases complexity).

To retrieve distance from the acquired signals using Eq. (31), the data processing chain must:

1. define the sweep range by choosing the initial and final frequency resonances;
2. determine the sweep range by measuring the number of Fabry-Pérot resonances within the sweep range;
3. measure the number of synthetic fringes (both integer and fractional part) within the sweep range;
4. calculate the number of fringes per resonance.

Data processing can be more efficient if all the available data is used. Instead of measuring only N and r to obtain N/r, we can measure the number of fringes N_i for each resonance r_i (where i represent the sequence of resonances) and determine N/r using a linear regression, thus reducing the uncertainty in the measurement, and making the procedure more robust to errors (we are making measurements at several tens of resonances instead of only two, the initial and the final).

The control, acquisition and data processing applications were all custom made, implemented in Labview™ from National Instruments. The system has the capability to do signal acquisition up to 5 MS/s (16 bits) and the output (for laser control) up to 4 MS/s (16 bits).

5.4 FSI sensor implementation and results

The first example of an FSI based sensor was designed to measure the OPD between two sub-telescopes of a multiple aperture optical telescope (Cabral & Rebordão, 2007). The implemented setup is sketched in Fig. 7. In the case of an absolute OPD measurement the result may be either positive or negative. The sign of the absolute OPD is thus required and must be measured. To overcome the ambiguity, a calibrated offset distance is created in arm A (A′ = A + Offset) of the interferometer (Fig. 7) ensuring that A′-B > 0, always, with the cost of increasing the maximum range (the Offset must be larger than half of the measurement range). The real distance difference is obtained by subtracting the calibrated Offset value.

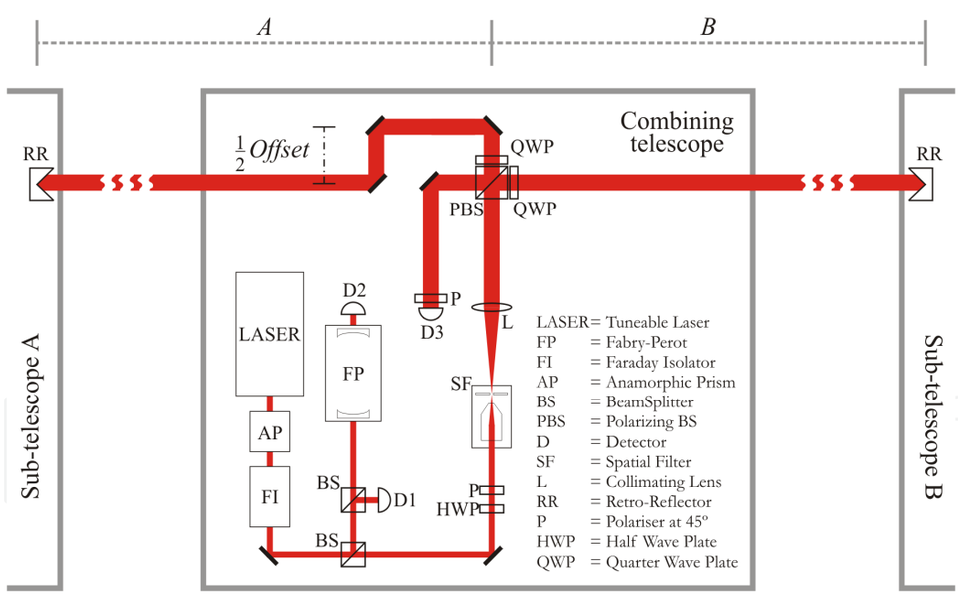

Fig. 7. Setup of the implemented FSI absolute sensor.

A Faraday isolator (FI) prevents feedback from the interferometer components back to the ECDL laser, and an anamorphic prism pair (AP) circularizes the elliptical cross section of the beam. The beam is then split by the first beam splitter (BS): one part is reflected to the sweep range & power monitoring measurement subsystems and the remainder is transmitted to the interferometer. A second BS splits the reflected beam into the power monitoring detector (D1) (reflected part) and the FP Interferometer that includes D2 (transmitted part). The beam

transmitted to the interferometer is filtered by the spatial filter (SF) and collimated by lens (L); before entering the interferometer, it goes through a half have plate (HWP) and a 45º oriented polarizer (P). These two elements enable the original vertical polarized light to be rotated by 45º. After the interferometer beam splitter, two quarter wave plates (QWP) transform the reflected vertical and transmitted horizontal polarized into circular polarized light that, after reflection in the retro-reflectors (RR) and another passage through the QWP, are redirected towards the detector (D3). Before the detector, a 45º polarizer (P) enables interferences.

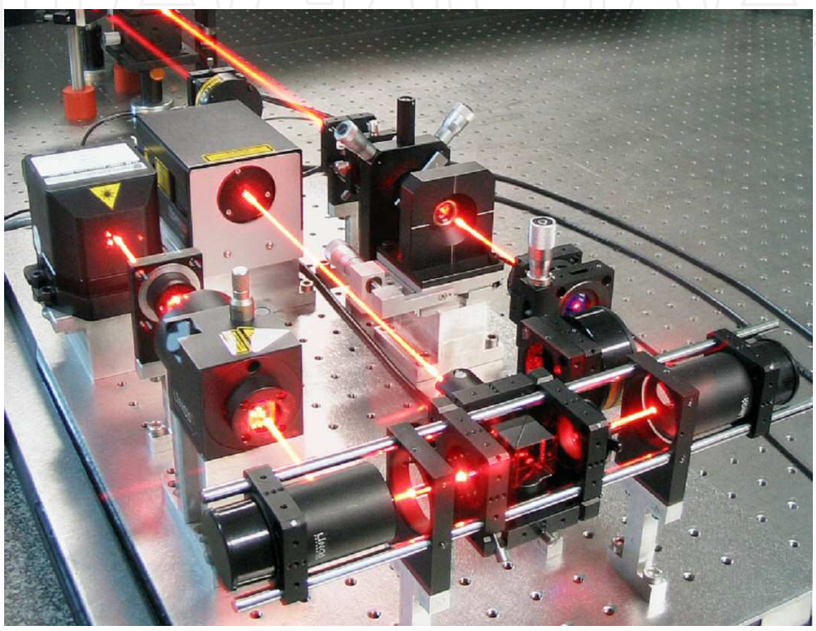

Fig. 8. FSI prototype implementation of the setup described in Fig. 6.

Fig. 8 shows a picture of the implemented prototype. The tunable laser is an ECDL capable of a mode-hop-free sweep range up to 150 GHz (TBL-7000 from NewFocus in a Littman-Metcalf mounting at 633 nm), corresponding to a synthetic wavelength down to 2 mm. The FP has a free spectral range of 1 GHz (TOPTICA high resolution, temperature stabilized, confocal Fabry-Pérot with a real finesse up to 1000). The FP was calibrated using the sensor hardware by means of two absolute measurements and a relative calibrated distance measurement between the two absolute positions, a kind of self-calibration (Cabral & Rebordão, 2006). This is a simple procedure and thus highly convenient to be implemented in space applications.

The graph in Fig. 9 shows the typical results obtained with this sensor. Each point corresponds to 200 consecutive measurements (with sweep duration of 100 ms) and a 2σ m for distances up to 1 m, increasing with distance as expected. Results confirm model predictions (continuous line) for $\delta N = 1/500$, $\delta FSR = 6$ kHz, and $\delta r = 1/3000$ (consequently $\delta\Lambda = 14$ nm). Measurement uncertainty is well below the 10 µm level.

Similar tests were performed for the dynamic mode that confirmed the efficiency of the compensation model, even in the presence of a non-constant drift speed (Cabral & Rebordão, 2007).

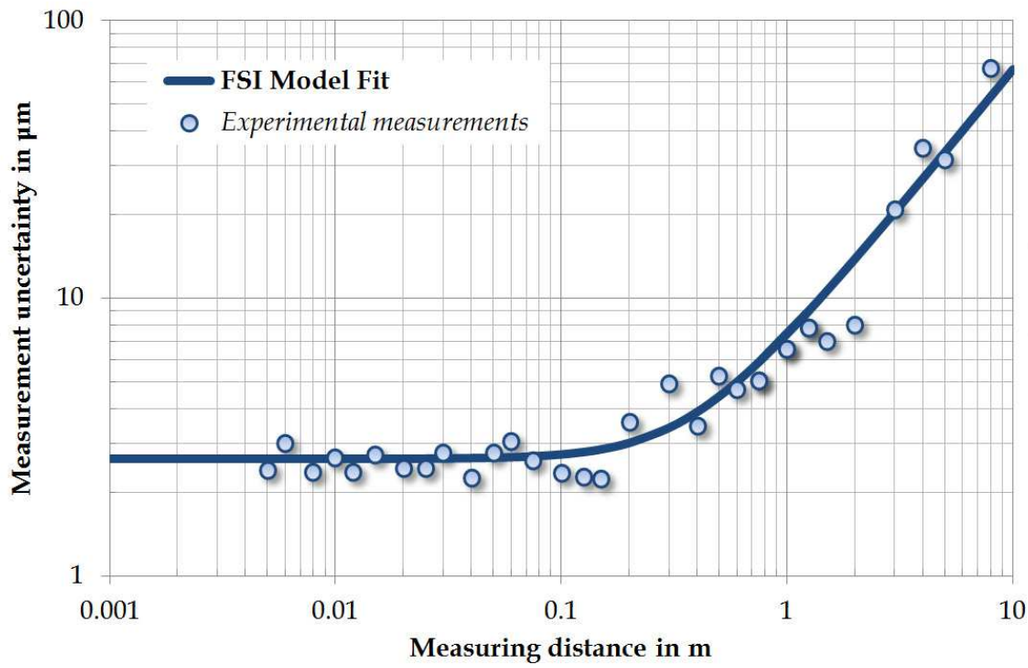

Fig. 9. FSI experimental measurements 2σ error in static a mode.

5.5 Dual FSI sensor implementation and results

The second example of an FSI based sensor makes use of the Dual FSI concept. The prototype was designed to measure at a nominal distance of 50 m, within a 10 m interval (Cabral et al., 2010). As mentioned previously, for such a distance, in a traditional FSI implementation (single interferometer mode), the uncertainty is dominated by the two uncertainty components related to the sweep range measurement and, to achieve accuracies below 100 µm it would be necessary to increase significantly the complexity of the FP subsystem. The Dual FSI approach overcomes this limitation without a major increase in the complexity, simply by adding a long reference fibre in the reference arm of a measurement interferometer and using an additional (reference) interferometer to calibrate the fibre.

In order to provide the sensor with assembly flexibility, the prototype implementation comprises three subunits, mechanically decoupled, with an optical connection implemented by fibres:

- Laser & Detection – Unit that contains the ECDL and the detectors for the two interferometers and the FP.
- FSI Head – Unit that includes the FP and the FSI interferometer(s) beam splitter (BS1 in Fig. 4).
- Optical Head – Optics that form the two interferometer arms.

Fig. 10 shows a picture of the Dual mode FSI sensor breadboard where is possible to identify the Laser & Detection, the FSI Head, the Optical Head unit and the long reference fibre housing.

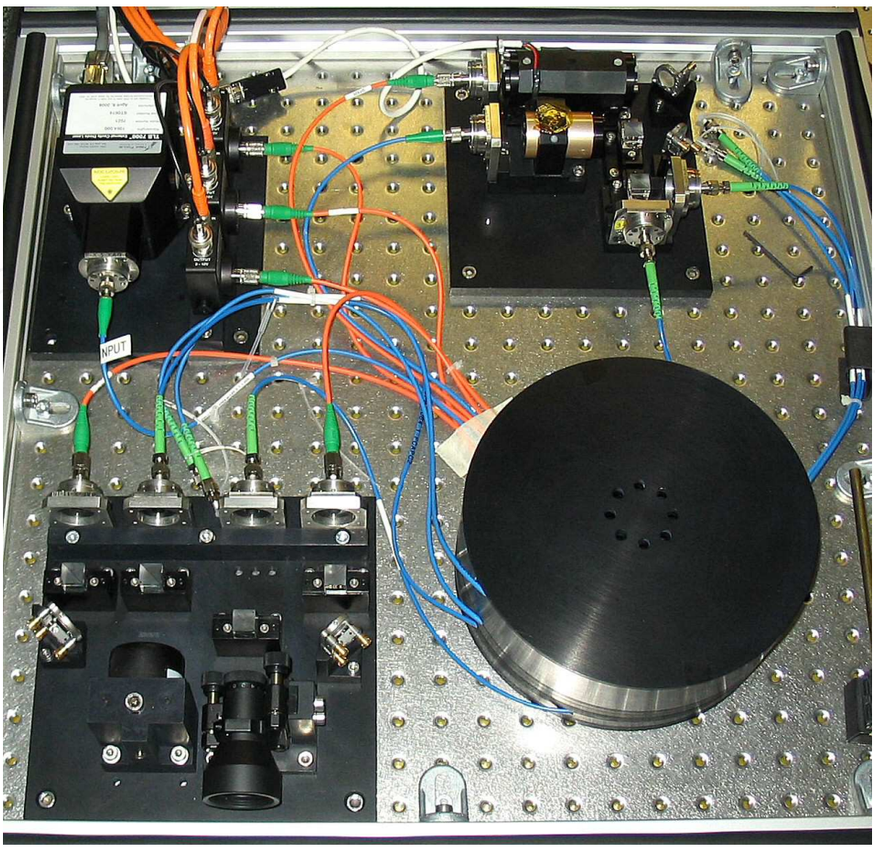

Fig. 10. Dual FSI sensor breadboard, showing Laser & Detection unit (top left), the FSI Head (top right), the Optical Head (bottom left) and the long reference fibre housing (bottom right).

In the Laser & Detection unit, the laser is the StableWave™ Model TLB-7021 by NewFocus, based on a Littman-Metcalf design (1024 nm). This ECDL is fibre pigtailed, and can achieve a maximum 85 GHz mode-hop-free frequency sweep, resulting in a minimum synthetic wavelength of 3.5 mm. In terms of sweep speed, it is possible to perform the complete sweep range in 50 ms, using a triangular shaped modulation, without noticing any major change in the laser response. The laser has a good stability in the short-term (μs), shorter than 50 kHz, but a poor stability performance at the medium-term (ms), having a direct impact in the sensor performance (disturbances caused by acoustically excited mechanical resonances in the laser cavity).

The FSI Head starts with a Faraday Isolator to prevent any residual back reflection into the laser as the ECDL behaviour is highly sensitive to feedback. Next, the light is split to the interferometers and the FP. As mentioned before, the FP has a critical impact in the system performances. An air spaced confocal etalon was manufactured (by IC Optical Systems Ltd) in Zerodur with a cavity length of 50 mm, corresponding to a FSR of 1.5 GHz. In terms of Finesse, the selected high reflectivity coating produces a very thin resonance peaks, experimentally measured to be, at least, 4700. The measured level of thermal stability (approximately 10 mK) corresponds to a FSR stability of a few tens of Hz, two orders of magnitude lower than the requirement in the uncertainty of the FSR.

After the beam splitter that directs half the light to the FP, the light is split again towards a small connection fibre and the long reference fibre, both already part of the interferometers arms. Both fibres are PANDA Polarization Maintaining (PM) with FC/APC connectors (low return loss). All the fibres are located in the fibre housing, shown in Fig. 11, to ensure mechanical stability and increase (by inertia) the short term thermal stability.

The length of the long reference fibre, used in the Dual FSI interferometers, must be twice the distance we want to subtract to the measuring range (while the light in the measurement path performs a round trip in the reference fibre it only travels in one direction). A 71 m fibre was selected, allowing an OPL subtraction of approximately 102 m (corresponding to the difference between the reference fibre length and the measurement arm fibre of 1 m multiplied by the refractive index of the fused silica). The setup of the Optical Head is slightly different from the one illustrated in Fig. 2, as in the reference interferometer an additional retro-reflector (RR_{REF}) allows the definition of the point from where the absolute measurement is referenced. Fig. 11 shows the optical setup of the implemented measurement (a) and reference interferometer (b). The position of the BS was chosen in order to make the measured OPD in the reference interferometer equal to the difference between the two fibres ($F_{REF} - F_{MEAS}$).

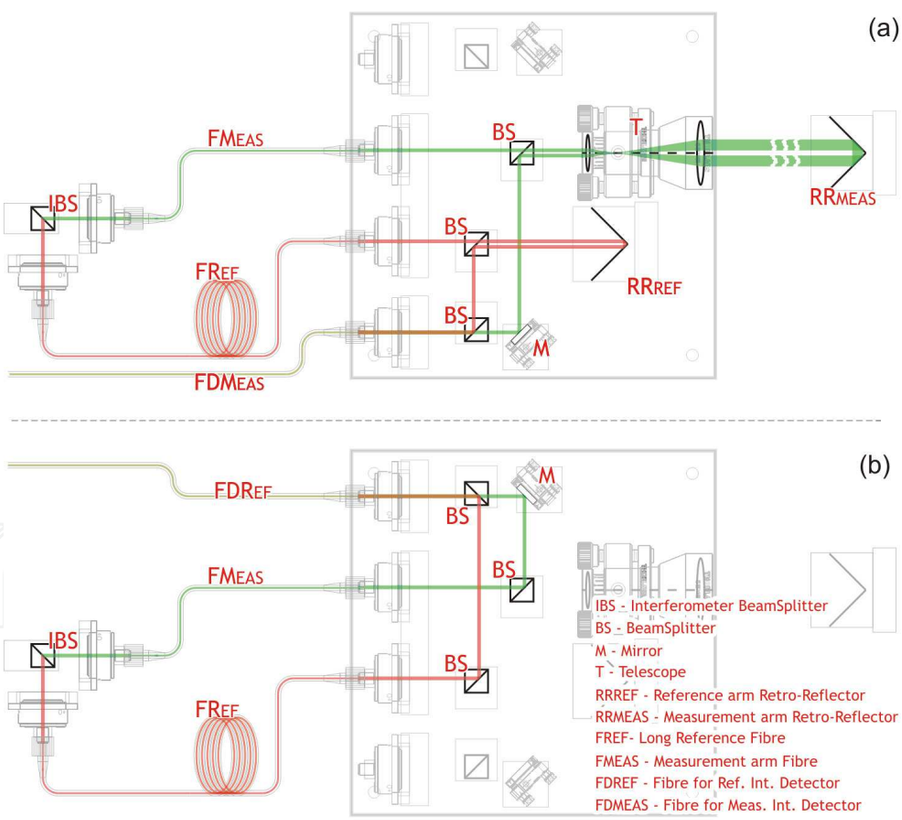

Fig. 11. The dual FSI measurement (a) and reference (b) interferometer.

The performances of the sensor result on the added contribution of the uncertainty in the reduced OPD measurement (by the measurement interferometer) and the long reference fibre calibration (by the reference interferometer).

The graph in Fig. 12 shows the results obtained with the contribution of the two mentioned uncertainty components. Each point corresponds to the 2σ dispersion (95% confidence interval) for 300 measurements. As shown, the contribution of the reduced OPD measurement is lower than 10 µm for the first few meters, and smaller than 30 µm for an absolute distance of 10 m.

To evaluate the component related with the calibration of the reference fiber, 2500 sequential measurements were performed, each with a duration of 100 ms. The measurement dispersion at 2σ was 554 µm for a mean value of 101 805 363 µm. The final uncertainty in the calibration of the fiber OPL is a function of the number of measurements that contribute to the calculated average length (and also the contribution of the FP FSR calibration uncertainty). The longer the duration of the calibration, the larger will be the decrease (by √N) of the uncertainty value resulting from the measurement dispersion. With a calibration period of 300 s (during which temperature was stable enough to consider a static OPL in the fibre), the uncertainty for the 101.8 m fibre OPL 31.2 µm (note that the contribution to the measured distance will be half of this value).

Fig.12 shows the uncertainty for the current dual FSI configuration using a 71 m fused silica fiber (101.8 m OPL) that allows a measurement range from 51 m to 61 m with accuracy smaller than 40 µm.

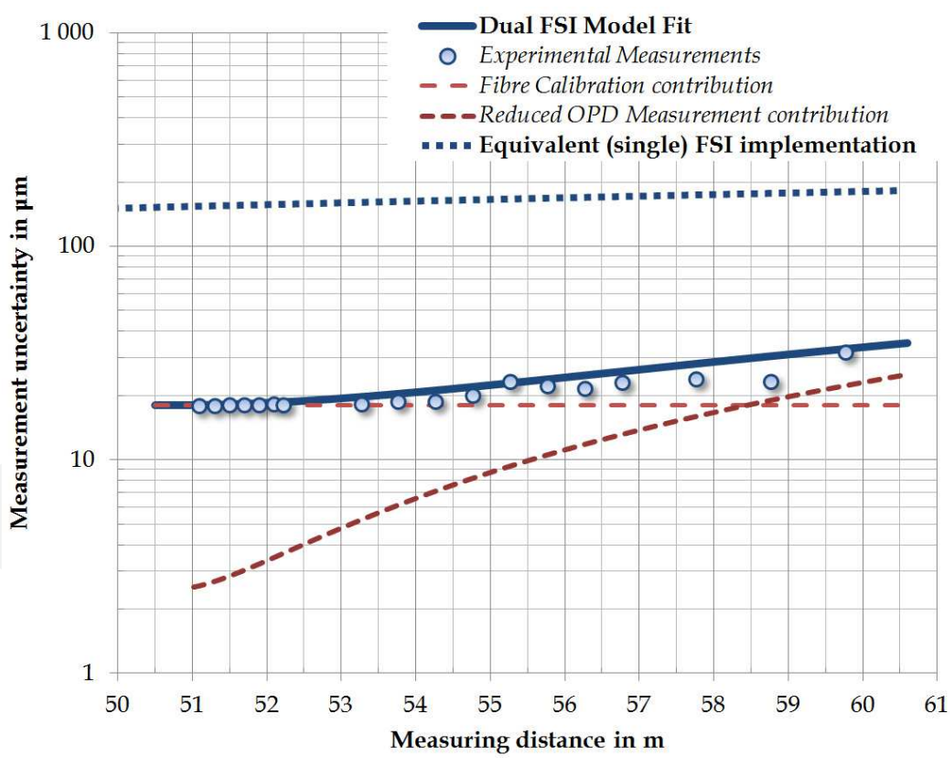

Fig. 12. Uncertainty for the current dual FSI configuration using a 71 m fused silica fibre (101.8 m OPL).

As it can be seen in Fig. 12, the improvements resulting from the Dual FSI concept compared to the expected results in a single FSI implementation are clear. Although the concept is

limited by configuration to specific range intervals (determined by the length of the reference fiber), the enhancement in the measurement accuracy is about one order of magnitude.

6. Conclusions

This chapter showed that FSI is a particularly versatile technique for absolute dimensional metrology, allowing different approaches for different applications with different needs, both in terms of range and accuracy.

The concept has a simple model, experimentally validated, the results of which are presented in this work. There is an excellent match between measurements and computer simulations.. The model proved to be sufficiently robust to allow the setup of the different parameters and implementation concepts for particular applications.

The most critical issue in the FSI technique is sensitivity to drift. Whilst in a laboratory with a controlled environments (temperature, pressure and vibrations) it is possible to achieve conditions where drift can be neglected, the same does not applies to the majority of the applications (like the example of space instrumentation). The case of FSI as a low complexity sensor requires self-sufficiency in terms of drift compensation. A drift compensation method using two consecutive measurements was also presented. In addition to the compensation of the error introduced by drift, the method was also provides an efficient way to measure drift speed, using exclusively the same set of data.

In terms of FSI performance, the accuracy at small distances is determined by the capability to interpolate a synthetic fringe. To improve accuracy we must choose the smallest possible synthetic wavelength, corresponding to the highest possible mode hop free frequency sweep range. The sweep range and the measurement frequency (which defines the sweep duration) determine the required frequency sweep rate. Even in an ECDL (currently the fastest tunable laser), the sweep rate should not exceed a few thousands of GHz/s, otherwise sweep non-linearities will jeopardise sensor performance. Therefore, even if the laser is capable of a larger sweep, the measurement frequency will limit the minimum synthetic wavelength. A smaller synthetic wavelength also decreases the influence of the drift because it decreases the amplification factor.

For large distances, accuracy is determined by the uncertainty in the synthetic wavelength value, as this will be propagated through the large number of synthetic fringes. As the synthetic wavelength is measured by counting the number of FSR in a FP, its uncertainty is determined by the stability of the FSR and also by how accurately the resonance peaks are located. Whenever the range is limited to a region around a large distance, it is possible to achieve high accuracy at large distance using a Dual FSI sensor approach, maintaining the reduced complexity inherent to the FSI technique.

Frequency sweeping interferometry is therefore an essential method for absolute distance metrology, especially when complexity and robustness are critical drivers (a must in space metrology). The flexibility of its parameterisation is an important advantage of the technique, allowing the same device to be used for a wide variety of mission requirements.

7. References

Amann, M.-C. & Buus, J. (1998). *Tunable Laser Diodes*, Artech House ISBN: 978-0890069639, 1998

Cabral, A. & Rebordão, J. (2005). Absolute distance metrology with frequency sweeping interferometry, *Recent Developments in Traceable Dimensional Measurements III*, J. Decker, Gwo-Sheng Peng; eds. Proc. SPIE 5879, 195-204, 2005

Cabral, A. & Rebordão, J. (2006). Calibration of the Fabry-Pérot free spectral range using a tunable laser in a Michelson interferometer, *Optical Engineering* 45, 1005, 2006

Cabral, A. & Rebordão, J. (2007). Accuracy of frequency sweeping interferometry for absolute distance metrology", *Optical Engineering* 46(07), 073602, 2007

Cabral, A. et al. (2009). Absolute distance metrology for long distances with dual frequency sweeping interferometry, *XIX IMEKO World Congress, Fundamental and Applied Metrology*, Lisbon, Portugal, 1942-1947, 2009

Cabral, A. et al. (2010). Dual-frequency sweeping interferometry for absolute metrology of long distances *Optical Engineering* 49, 085601, August 2010

Calvel, B. et al. (2004). High Precision Optical Metrology for DARWIN, *2nd Int. Symposium on Formation Flying Missions and Technologies*, Arlington, VA, USA, 14-16, 2004

Coe, P. A. et al. (2004). Frequency scanning interferometry in ATLAS: remote, multiple, simultaneous and precise distance measurements in a hostile environment, *Measurement Science and Technology*, vol. 15, pp. 2175–2187, 2004

Dändliker, R. et al. (1988). Two-wavelength laser interferometry using superheterodyne detection, *Optical Letters.* 13(5), 339-341, 1988

Dändliker, R. et al. (1995). High-accuracy distance measurements with multiple-wavelength interferometry, *Optical Engineering* 34(8), 2407-2412, 1995

Edwards, C. S. et al. (2000). Experimental verification of a swept-frequency laser interferometer for distance measurement, *NPL Report* CBTLM 4, 2000

Hecht, J. (2001). Tuning in to tunable lasers, *Laser Focus World*, pp.121-125, 2001

IOS (1995). Guide to the Expression of Uncertainty in Measurement, *International Organization for Standardization*, Geneva, Switzerland, 1995

Kikuta H. et al. (1986). Distance measurement by the wavelength shift of laser diode light, *Applied Optics*, vol. 25(17), pp.2976-2986, 1986

Kinder, Th. & Salewski, K. D. (2002). Absolute distance interferometer with grating-stabilized tunable diode laser at 633 nm, *Journal of Optics A*, 4, S364-S368, 2002

Stone, J. et al (1999). Absolute interferometry with a 670-nm external cavity diode laser, *Applied Optics* vol.38(28), pp.5981-5994, 1999

Swinkels, B. et al. (2005). Absolute distance metrology for space interferometers, *Recent Developments in Traceable Dimensional Measurements III*; Jennifer E. Decker, Gwo-Sheng Peng; eds. Proc. SPIE 5879, 216-222, 2005

Thiel, J. et al. (1995). Interferometric measurement of absolute distances of up to 40 m, *Measurement* vol.16, pp.1-6, 1995

Vaughan, J.M. (1989). *The Fabry-Pérot Interferometer: History, Theory, Practice and Applications*, Institute of Physics Publishing, ISBN: 978-0852741382, 1989

Yang, H. J. et al. (2005). High-precision absolute distance and vibration measurement with frequency scanned interferometry, *Applied Optics*, 44(19), 3937-3944, 2005

Stone, J. & Zimmerman, J. (2004). Engineering metrology toolbox, refractive index of air calculator *NIST*, http://emtoolbox.nist.gov/Wavelength/Documentation.asp, 2004

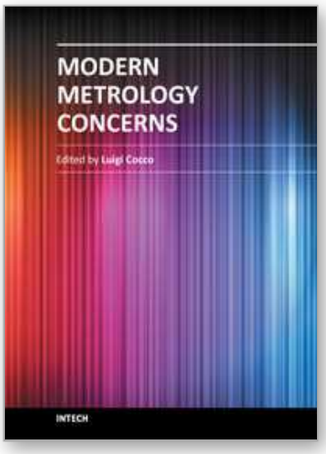

Modern Metrology Concerns

Edited by Dr. Luigi Cocco

ISBN 978-953-51-0584-8
Hard cover, 458 pages
Publisher InTech
Published online 16, May, 2012
Published in print edition May, 2012

"What are the recent developments in the field of Metrology?" International leading experts answer this question providing both state of the art presentation and a road map to the future of measurement science. The book is organized in six sections according to the areas of expertise, namely: Introduction; Length, Distance and Surface; Voltage, Current and Frequency; Optics; Time and Relativity; Biology and Medicine. Theoretical basis and applications are explained in accurate and comprehensive manner, providing a valuable reference to researchers and professionals.

How to reference

In order to correctly reference this scholarly work, feel free to copy and paste the following:

Alexandre Cabral, José Manuel Rebordão and Manuel Abreu (2012). Dimensional Metrology and Frequency Sweeping Interferometry, Modern Metrology Concerns, Dr. Luigi Cocco (Ed.), ISBN: 978-953-51-0584-8, InTech, Available from: http://www.intechopen.com/books/modern-metrology-concerns/dimensional-metrology-and-frequency-sweeping-interferometry

INTECH
open science | open minds

InTech Europe
University Campus STeP Ri
Slavka Krautzeka 83/A
51000 Rijeka, Croatia
Phone: +385 (51) 770 447
Fax: +385 (51) 686 166
www.intechopen.com

InTech China
Unit 405, Office Block, Hotel Equatorial Shanghai
No.65, Yan An Road (West), Shanghai, 200040, China
中国上海市延安西路65号上海国际贵都大饭店办公楼405单元
Phone: +86-21-62489820
Fax: +86-21-62489821